LoRa and Rotating Polarization Wave: Physical Layer Principles and Performance Evaluation

Zaid Ahmad, Shaiful J. Hashim, Guillaume Ferre, Fakhrul Z. Rokhani, S. A. R. Al-Haddad, Aduwati Sali

IEEE Access
Multidisciplinary | Rapid Review | Open Access Journal

Received 20 December 2022, accepted 26 January 2023, date of publication 3 February 2023, date of current version 16 February 2023.

Digital Object Identifier 10.1109/ACCESS.2023.3242552

RESEARCH ARTICLE

LoRa and Rotating Polarization Wave: Physical Layer Principles and Performance Evaluation

ZAID AHMAD[1,2], (Member, IEEE), SHAIFUL J. HASHIM[2], GUILLAUME FERRÉ[3], (Senior Member, IEEE), FAKHRUL Z. ROKHANI[2], (Member, IEEE), S. A. R. AL-HADDAD[2], (Senior Member, IEEE), AND ADUWATI SALI[2,4], (Senior Member, IEEE)

[1]Department of Electrical and Computer Engineering, COMSATS University (CUI), Lahore, Punjab 54000, Pakistan
[2]Department of Computer and Communication Systems Engineering, Faculty of Engineering, Universiti Putra Malaysia (UPM), Serdang, Selangor 43400, Malaysia
[3]IMS Lab, University of Bordeaux, 33405 Talence CEDEX, France
[4]WiPNET Research Centre, Department of Computer and Communication Systems Engineering, Faculty of Engineering, Universiti Putra Malaysia (UPM), Serdang, Selangor 43400, Malaysia

Corresponding authors: Zaid Ahmad (zaidahmad.r@gmail.com), Shaiful J. Hashim (sjh@upm.edu.my), and Guillaume Ferré (guillaume.ferre@u-bordeaux.fr)

ABSTRACT Link reliability and enhanced coverage are the primitive concerns of Low-Power Wide-Area Networks (LPWANs) for suitability to critical Internet of Things (IoT) applications. Reliability is limited by the destructive multipath propagation, data rate and sensitivity, that ultimately limits the coverage range. LoRa by far is the predominant LPWAN operating on unlicensed spectrum. Despite its robust Chirp Spread Spectrum (CSS) modulation, there is a severe degradation in its error performance particularly in hostile propagation environments, and an excessive reduction in coverage. Rotating Polarization Wave (RPW) is a potential LPWAN recently emerged to achieve a highly reliable IoT and Machine-to-Machine (M2M) communication. This is the first paper to provide comprehensive error performance comparison between LoRa and RPW. Okumura-Hata model is used for median path loss calculation. Shadowing and fast fading margins of RPW and LoRa are estimated. Effective gain of RPW is computed from error performance. Results have shown that LoRa offers a sensitivity of 23 dB higher than RPW under AWGN conditions. However, under fading conditions, RPW exhibits a sensitivity of 15 dB higher than LoRa. At a reference distance of 100 m, the maximum received signal strength of RPW is −39 dBm, which is 29 dB above LoRa. The maximum coverage distance attained by RPW is 15 km, which is 1.5 times of LoRa.

INDEX TERMS IoT, link budget, LoRa, LPWAN, multipath fading, Okumura-Hata, polarization diversity, RPW, shadowing.

I. INTRODUCTION

Low-Power Wide-Area Network (LPWAN) technologies have spurred in the last decade, and most of them have been commercialized. They can be categorized as cellular LPWANs and unlicensed band LPWANs. In most of the unlicensed band LPWANs, the physical layer is proprietary while MAC and upper layers have been standardized and are open for improvement. LPWAN arena is primarily dominated by four LPWANs: LoRa, Sigfox, NB-IoT and LTE-M [1]. LoRa and Sigfox operate on unlicensed spectrum while NB-IoT and LTE-M are cellular LPWANs. LoRa is the leading LPWAN with a projected growth of 660 million connections by 2023 [1]. It offers high reliability, high sensitivity, extended coverage, large link budget and greater energy efficiency [2]. However, with the advent of Rotating Polarization Wave (RPW) LPWAN [3], [4], Internet of Things (IoT) market is expected to witness an interesting competition between RPW and other LPWANs. Early simulation results have shown that RPW is very reliable in an extremely hostile

The associate editor coordinating the review of this manuscript and approving it for publication was Walid Al-Hussaibi.

propagation environment [3], [5]. This has motivated the authors to further investigate the performance comparison of LoRa and RPW, and to the best of the knowledge of authors, this is the first paper to provide comprehensive error performance comparison between LoRa and RPW for LPWAN connectivity.

LoRa has sufficiently matured over the past decade and gained much attention in the LPWAN market. Latest research trends in LoRa include reliability, scalability, and adaptive resource allocation [6]. LoRa has a proprietary physical layer (PHY) named after it, and an open-standard MAC layer, known as LoRaWAN. RPW, on the other hand, is going through its embryonic stages. Its PHY is currently owned by Hitachi (Japan) while its MAC has been defined but not implemented [7]. Improvements are underway in data rate [3] and reliability for various propagation conditions.

Reliability is one of the major challenges for LPWANs. IoT applications like industrial monitoring and control, M2M communication and telemetry demand a minimum reliability of 99.99 percent in terms of packet delivery [8]. Multipath fading is central to the quality of link in urban as well as forest areas as it has a huge impact on the link reliability [9]. In urban areas, it is caused by reflectors and scatterers in the vicinity of transmitters and receivers; while in forests, the underlying causes are vegetation, climate variation, and Non-Line-of-Sight (NLoS) conditions. Many papers reported that trees, leaves and foliage in tropical environments can attenuate wireless signal by 15 to 30 dB on VHF and UHF frequencies [10], [11], [12].

Severe degradation in error performance of LoRa has been reported due to multipath effects [13], [14]. The performance can be improved by use of higher spreading factors (SF) of 10 to 12 but at the expense of reduction in transmission rate. On the other hand, RPW is less sensitive to multipath fading, and has a significant advantage over LoRa in terms of bit error rate (BER) [5]. This can be attributed to the reception of information signal at a large number of redundant polarizations and hence minimize depolarization and multiple reflections caused by surrounding objects. However, this feature of RPW to combat multipath fading needs further investigation to establish its use as LPWAN.

Being the leader in IoT LPWANs, LoRa was originally designed to reach a theoretical coverage range of 5 km in urban and 15 km in rural areas [9]. However, despite its robust Chirp Spread Spectrum (CSS) modulation, presence of obstacles and reflectors desperately affects the performance. Factors such as reflection and absorption by obstacles reduce the real-world range of communication [15]. Varying the height of antenna affects the coverage and antenna orientation affects communication range [16]. This suggests that the polarization of the antenna and the signal has its role in extended coverage and range. Spreading factor and antenna orientation also affect the signal quality [16]. The practical range drastically reduces to 200 m in urban scenario with high-density buildings and greater human activity [9]. Similarly, in temperate forest, LoRa can establish a communication link with a range of 250 m only. Slightly different results for an urban range (500 m) are obtained in [2]. A trade-off among SF, sensitivity and data rate [15] shows that decreasing SF from 12 to 6 enhances the data rate from $\approx$0.3 kbps to $\approx$10 kbps (30x), but the sensitivity is reduced by almost 100 times (100x) [15]. Consequently, Time-on-Air (ToA) is significantly increased and the battery life is affected. The degradation of receiver sensitivity eventually translates into reduced communication range. While most of the recent research on LoRa focuses on adaptive SF allocations, tuning the parameters to ensure successful reception at the cost of data rate is sometimes not recommended. For example, the limited bandwidth in LoRa modulation makes it less suitable for high bit rate data transfer from devices like image sensors [17]. Another special case is the communication link for the fringe or edge coverage [18]. In such cases, faster PHY setting i.e. higher data rates and shorter ToA with re-transmissions are required to improve packet reception rate and link quality. This approach translates to improved energy efficiency. Therefore, a careful PHY and RF design can help provide extended range.

In view of the limitations and trade-offs stated above, RPW is expected to outperform LoRa. RPW signal can reach farther than LoRa because of more resilience to multipath, since polarization can be controlled. Also it offers higher data rate, and therefore more energy-efficiency. Generally, the previous works on LoRa link budget analysis have not incorporated LoRa processing gain on account of spectral spreading. Furthermore, no previous work has investigated the range of RPW in different terrains particularly urban, suburban, and rural. Shadowing and multipath fading are major contributors to the path loss, and it is crucial to include shadowing and fast fading margins into the link budget computations [19]. But, previous works on LPWANs have either ignored fast fading margin or have used empirical values for shadowing and fast fading margins [2], [20]. Rather, miscellaneous variable obstacle losses have been considered [2]. Therefore, generalization about LPWAN link performance cannot be made from the existing literature. Since RPW prototype has not been tested for different propagation environments, a comparison between RPW and LoRa using statistical estimates for fade margins is also essential. Other losses such as fixed obstacle losses on top of a uniform gently rolling terrain also occur. Moreover, outdoor-to-indoor loss should also be considered to accommodate deep indoor coverage of an IoT end device (ED) [20]. Hence a rigorous performance comparison of RPW and LoRa based on the gaps highlighted above is inevitable.

The objective of this paper is to evaluate the PHY performance of LoRa and RPW over a point-to-point link. This has been achieved through the following contributions:

1) Continuous-time mathematical models are proposed to illustrate physical layer principles of RPW and LoRa
2) Empirical models of RPW and LoRa are employed for link budget analysis

3) Fast fading margins are incorporated into link budget analysis of RPW and LoRa to determine their receiver sensitivity (ρ), received signal strength (RSS) and maximum coverage range ($R_{\max}$).

The remaining paper has been organized as follows: Section II mathematically describes the principles of RPW and LoRa modulation and detection. Empirical models for BER analysis are depicted in Section III. Section IV comprehensively covers the determination of link parameters and their impact on performance in terms of sensitivity, fade margins, path loss, gains and miscellaneous losses. Simulation results of RSS and $R_{\max}$ have been presented and discussed for urban, suburban and rural areas. Section V summarizes the important results and comparative performance of the two LPWANs, and Section VI concludes the paper.

II. PHYSICAL LAYER PRINCIPLES

This section gives a comprehenstive mathematical treatment of RPW and LoRa for their respective modulation and detection principles.

A. PRINCIPLES OF RPW

RPW is the rotation of binary symbols in polarization domain to improve the reliability of wireless link. The binary information flow generated from the MAC layer is divided into k-bit symbols $m_i \in \{0, M-1\}$, where $M = 2^k$ is the total number of possible symbols. RPW signal is generated using Rotating Polarization Multi-level Phase-Shift Keying (RP-MPSK) modulation that is capable of slowly varying the polarization of the electromagnetic wave with time over an entire symbol period T_s [3]. This is illustrated in Fig. 1 in terms of horizontal and vertical polarized components.

First, a 'so-called' dual MPSK modulation is performed on a symbol that results in two equivalent baseband MPSK waveforms $c(t)$ and $s(t)$, given by

$$c(t) = \pm\sqrt{2}\cos(2\pi f_b t + \varphi_i), \tag{1a}$$

$$s(t) = \pm\sqrt{2}\sin(2\pi f_b t + \varphi_i), \tag{1b}$$

where $f_b = 1/T_s$ is the baseband modulation frequency, and $\varphi_i = \frac{2\pi m_i}{M} + \phi_{\text{ini}}$ is the phase corresponding to the i^{th} symbol m_i transmitted at time iT_s, with ϕ_{ini} as the initial phase of the MPSK constellation (when $m_i = 0$). The pair of signals in (1) can alternatively be expressed as a complex exponential signal $g(t)$ of the form

$$g(t) = \sqrt{2} \cdot e^{j(2\pi f_b t + \varphi_i)}, \tag{2}$$

so that

$$c(t) = \Re\{g(t)\} \quad \text{and} \quad s(t) = \Im\{g(t)\}. \tag{3}$$

where $\Re\{\cdot\}$ and $\Im\{\cdot\}$ denote the real and the imaginary parts, respectively. The complex envelope of the baseband signal $g(t)$ is given by

$$m(t) = \sum_{i\in\mathbb{Z}} g(t - iT_s) \tag{4}$$

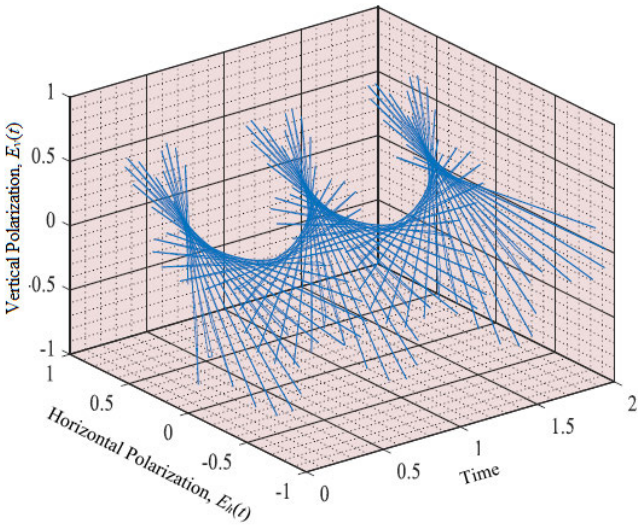

FIGURE 1. Illustration of RPW signal.

The signal is then up-converted to complex radio signal $q(t)$ of carrier frequency $f_c \gg f_b$ as

$$q(t) = m(t)\cos(2\pi f_c t) \tag{5}$$

The real part of $q(t)$ is transmitted through horizontally polarized antenna as $h_t(t)$ and the imaginary part is transmitted through vertically polarized antenna as $v_t(t)$

$$h_t(t) = \Re\{q(t)\} \quad \text{and} \quad v_t(t) = \Im\{q(t)\}. \tag{6}$$

Eventually, the electromagnetic RPW signal takes the form

$$\Phi_{\text{RPW}}(z,t) = \Re\{m(t)\}u_c(t)\mathbf{a}_x + \Im\{m(t)\}u_c(t)\mathbf{a}_y, \tag{7}$$

where $u_c(t) = \cos(2\pi f_c t + \beta z)$ is the carrier signal with phase constant $\beta = 2\pi/\lambda$, $\mathbf{a}_x$ and $\mathbf{a}_y$ are the unit vectors along horizontal and vertical polarizations respectively, λ is the wavelength, and RPW travels along z-axis. For Nyquist ideal filtering, the bandwidth of $q(t)$ is $B = f_b = R_s = R_b/k$, with R_s and R_b denoting symbol rate and bit rate, respectively [21].

Assuming perfect time and phase synchronization, signals $h_r(t)$ and $v_r(t)$ received from horizontal and vertical polarized antennas respectively, are sampled at a rate $f_p = 1/T_p = N_p f_b$, with $f_b < f_p \ll f_c$:

$$h_r(nT_p) = h_c \cdot h_t(nT_p) + w_c(nT_p) \tag{8a}$$

$$v_r(nT_p) = h_s \cdot v_t(nT_p) + w_s(nT_p) \tag{8b}$$

Here, $h_c \sim \mathcal{N}_{\mathbb{C}}(0, \sigma^2_{h_c})$ and $h_s \sim \mathcal{N}_{\mathbb{C}}(0, \sigma^2_{h_s})$ are single-tap block fading channels. The complex circular white Gaussian noise signals are represented by $w_c(iT_r) \sim \mathcal{N}_{\mathbb{C}}(0, \sigma^2_{w_c})$ and $w_s(iT_r) \sim \mathcal{N}_{\mathbb{C}}(0, \sigma^2_{w_s})$. $N_p \in \mathbb{Z}$ is the sampling ratio, which is a parameter of primary interest in RPW as the order of polarization diversity increases with N_p.

The digital demodulation of r^{th} transmit symbol occurring over the interval $(rT_s - \frac{T_s}{2} \le t < rT_s + \frac{T_s}{2})$ corresponds to the processing of consecutive $N_p = \frac{T_s}{T_p}$ samples of (8):

$$r_h(\ell T_p) = h_r(\ell T_p + rT_s) \cdot \cos(2\pi f_b \ell T_p) \tag{9a}$$

$$r_v(\ell T_p) = v_r(\ell T_p + rT_s) \cdot \sin(2\pi f_b \ell T_p) \tag{9b}$$

Here, $\ell \in [0, N_p - 1]$. In this interval, all other terms in (4) vanish. Therefore,

$$h_r\left(\ell T_p + rT_s\right) = h_c \cdot \Re\left\{m(\ell T_p)\right\} + w_c^r\left(\ell T_p\right), \quad (10a)$$
$$v_r\left(\ell T_p + rT_s\right) = h_s \cdot \Im\left\{m(\ell T_p)\right\} + w_s^r\left(\ell T_p\right), \quad (10b)$$

where $m\left(\ell T_p\right) = \exp\left(j2\pi f_b\left[\ell Tp + \frac{m_r}{M} Ts\right]\right)$ using (4) and $w_{(\cdot)}^r(\ell T_p) = w_{(\cdot)}(\ell T_p + rT_s)$. Now combining (9) and (10), we obtain

$$r_h\left(\ell T_p\right) = x_h\left(\ell T_p\right) + w_h\left(\ell T_p\right), \quad (11a)$$
$$r_v\left(\ell T_p\right) = x_v\left(\ell T_p\right) + w_v\left(\ell T_p\right). \quad (11b)$$

The information terms are given by

$$x_h\left(\ell T_p\right) = h_c \cdot \Re\left\{m(\ell T_p)\right\} \cos\left(2\pi f_b \ell T_p\right), \quad (12a)$$
$$x_v(\ell T_p) = h_s \cdot \Im\left\{m(\ell T_p)\right\} \sin\left(2\pi f_b \ell T_p\right), \quad (12b)$$

and the noise terms are

$$w_h\left(\ell T_p\right) = w_c^r(\ell T_p) \cos\left(2\pi f_b \ell T_p\right), \quad (13a)$$
$$w_v\left(\ell T_p\right) = w_s^r(\ell T_p) \sin\left(2\pi f_b \ell T_p\right). \quad (13b)$$

The pair of signals in (11) is co-phased and combined using equal-gain combining (EGC). The advantage of EGC over selection combining (SC) is the increase in carrier-to-noise ratio (CNR), that increases with number of diversity branches [22]. Maximal ratio combining (MRC) can also be performed but the complexity increases because of the different weights assigned to each diversity branch. In EGC, all the branches are equally weighted. EGC is preferred over MRC because the CNR of EGC is only slightly less than MRC [22]. Employing EGC, the combined received sequence is given by:

$$r\left(\ell T_p\right) = r_h\left(\ell T_p\right) e^{-j\theta_h} + r_v\left(\ell T_p\right) e^{-j\theta_v} \quad (14)$$

Here θ_h and θ_v are the estimated phases of h_c and h_s, respectively. Assuming coherent detection, the m^{th} correlator can be expressed as

$$z_m\left(\ell T_p\right) = \cos\left(2\pi f_b[\ell T_p + \frac{m}{M} T_s]\right). \quad (15)$$

If $\mathbf{r}$ is the complex random vector associated with $r\left(\ell T_p\right)$ and $\mathbf{z}_m$ is the complex vector associated with $z_m\left(\ell T_p\right)$ the maximum likelihood sequence estimation (MLSE) is performed to detect the transmitted symbol m_r as

$$\hat{m}_r = \underset{m}{\text{argmax}}\ \Re\{\mathbf{r}\mathbf{z}_m^H\}, \quad (16)$$

where $(\cdot)^H$ represents Hermitian transpose. After all the transmitted symbols are detected, they are converted back to k-bit symbols and MAC bit-stream is recovered.

An equivalent discrete description of RPW generation and detection using RP-MPSK modulation is provided in [3].

It is important to note that RPW involves three different frequencies: the carrier frequency f_c, the polarization rotation frequency f_b (which is also RP-MPSK modulation frequency), and the sampling frequency f_p (at which RPW signal is sampled on receiver side, so that multiple polarizations of a symbol are obtained) that can be varied according to the required number of polarization samples of RPW signal. The higher the value of f_p keeping f_b constant implies improved signal recovery, and hence higher reliability. The relationship between these frequencies can be given as $f_b < f_p \ll f_c$. It is notable that f_p should be kept sufficiently small than f_c for successful RP-MPSK and maintain RPW characteristics over the channel. The modulation frequency f_b is fixed at 125 kHz because it is used by existing RPW prototype as well as LoRa modules [23], [24].

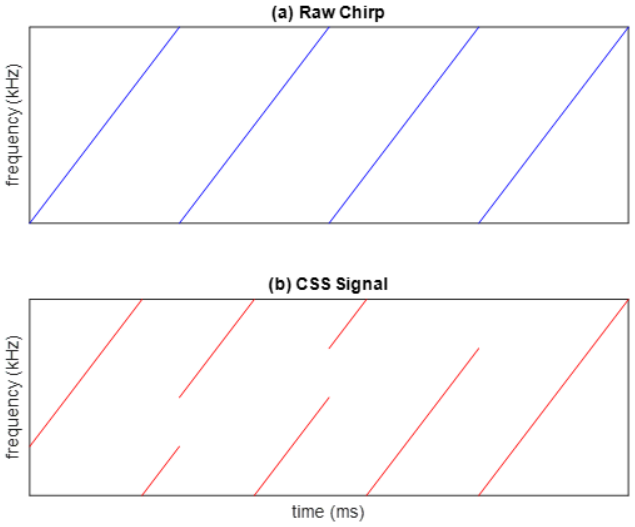

FIGURE 2. Illustration of (a) Raw chirp signal (b) LoRa CSS signal.

The sampling ratio $N_p = f_p/f_b$ is an important RPW parameter that impacts the reliability of communication. The minimum value of N_p is 3. This is a preliminary lower bound for the performance evaluation and validation of RPW. RP-MPSK demodulation is not guaranteed if $N_p < 3$, because RP-MPSK demodulation depends on the most frequently occurring symbol within a symbol period T_S of transmission. Per contra, any upper bound for N_p is not available in literature. Moreover, depending on the receiver hardware, the value of N_p can be as high as 32 or greater if ADC on receiver can support a sampling rate up to 4 Msps. This is subject to the baseband modulation frequency f_b.

B. PRINCIPLES OF LoRa

LoRa employs multiple spreading factors (SF) for improvement in range and energy efficiency, and to control bit rate [25]. The bit stream generated from MAC layer is divided into smaller sequences of length SF $\in [7 \ldots 12]$. Each small sequence is considered as a symbol, resulting in $M = 2^{\text{SF}}$ number of symbols. The spreading factor SF is the ratio of bit rate R_b to the symbol rate R_s, i.e. SF $= R_b/R_s$. Spread spectrum signal is generated by modifying a raw or reference chirp signal. The latter is defined as a signal whose frequency varies linearly with time over an entire symbol period T_s. The raw chirp can be an up-chirp or a down-chirp, depending upon whether its derivative is positive or negative, respectively.

An up-chirp is shown in Fig. 2a. The complex envelope of raw chirp for the interval $t \in \left[-\frac{T_s}{2}, \frac{T_s}{2}\right)$ can be expressed mathematically as follows:

$$c(t) = e^{j\theta_c(t)}, \quad \text{with } \theta_c(t) = \pm\pi \frac{B}{T_s} t^2, \tag{17}$$

where the transmitted chirp traverses through B Hertz. Furthermore, the '+' sign indicates an up-chirp and the '−' sign indicates a down-chirp. The variable frequency $f_c(t)$ during this traversal can be given by:

$$f_c(t) = \frac{1}{2\pi}\frac{d\theta_c(t)}{dt} = \pm\frac{B}{T_s} t. \tag{18}$$

Unlike digital communication systems without spectral spreading, where the symbol rate R_s is proportional to bandwidth, the signal bandwidth of LoRa CSS modulation is fixed to B having the following relationship with T_s:

$$M = B \times T_s. \tag{19}$$

Since each LoRa symbol must be unique, M orthogonal chirps are defined and mapped to respective M orthogonal symbols, so that each unique symbol m maintains a specific instantaneous phase trajectory.

Let the i^{th} symbol $m_i \in \{0, \ldots, M-1\}$ be transmitted at time iT_s. Then the up or down chirp associated with it is defined by introducing a delayed $\tau_i = \frac{m_i}{B}$ with its segment occurring outside the interval $[-\frac{T_s}{2}, \frac{T_s}{2})$ cyclically shifted back into $[-\frac{T_s}{2}, -\frac{T_s}{2} + \tau_i)$. This is the fundamental idea of LoRa modulation. It ensues that the modulated chirp corresponding to m_i is formulated in two segments:

1) a raw chirp advanced by $(T_s - \tau_i)$ for $t \in \left[-\frac{T_s}{2}, -\frac{T_s}{2} + \tau_i\right)$, and
2) a raw chirp delayed by τ_i for $t \in \left[-\frac{T_s}{2} + \tau_i, \frac{T_s}{2}\right)$.

For example, if it was an up-chirp, it will be expressed as:

$$f_c^i(t) = \frac{B}{T_s}(t - \tau_i) + B \quad \text{for } t \in \left[-\frac{T_s}{2}, -\frac{T_s}{2} + \frac{m_i}{B}\right)$$
$$f_c^i(t) = \frac{B}{T_s}(t - \tau_i) \quad \text{for } t \in \left[-\frac{T_s}{2} + \frac{m_i}{B}, \frac{T_s}{2}\right).$$

Fig. 2b is an illustration of modulated chirps. In terms of instantaneous phase:

$$\theta_c^i(t) = \pi\left[\frac{B}{T_s}(t - 2\tau_i)t + 2Bt\right] \quad \text{for } t \in \left[-\frac{T_s}{2}, -\frac{T_s}{2} + \frac{m_i}{B}\right)$$
$$\theta_c^i(t) = \frac{\pi B}{T_s}(t - 2\tau_i)t \quad \text{for } t \in \left[-\frac{T_s}{2} + \frac{m_i}{B}, \frac{T_s}{2}\right).$$

Eventually, the complex envelope of the transmitted signal is:

$$s(t) = \sum_{i\in\mathbb{Z}} e^{j\theta_c^i(t - iT_s)} \mathbb{1}_{\left[\frac{T_s(2i-1)}{2}, \frac{T_s(2i+1)}{2}\right]}(t) \tag{20}$$

where $\mathbb{1}_{[a,b]}(t)$ is the indicator function of the interval $[a, b]$ and $\theta_c^i(t)$ corresponds to the phase of the modulated chirp related to symbol m_i, which is transmitted at time iT_s.

For a perfect synchronization in time and frequency, and channel with single-tab impulse response $h \sim \mathcal{N}_{\mathbb{C}}(0, \sigma_h^2)$, the received signal sampled at rate T_e and denoted by $y(nT_e)$ can be written as

$$y(nT_e) = h \times s(nT_e) + w(nT_e), \tag{21}$$

where $w(nT_e) \sim \mathcal{N}_{\mathbb{C}}(0, \sigma^2)$ represents the complex noise assumed white, Gaussian and circular.

According to the patent EP2449690 [26], the transmitted symbols are detected by multiplying every time frame with T_s duration of the received signal complex envelope by the conjugate version of the raw chirp (17) used in the transmitter (up or down). Thus the digital demodulation of the p^{th} transmitted symbol ($pT_s - \frac{T_s}{2} \le t < pT_s + \frac{T_s}{2}$) corresponds to the processing of $N = \frac{T_s}{T_e}$ samples:

$$r_p(nT_e) = y(nT_e + pT_s)e^{-j\theta_c(nT_e)}, \tag{22}$$

with $n \in [\![-\frac{N}{2}, \frac{N}{2} - 1]\!]$. In this interval, all the terms of the sum in (20) are null, except the term $i = p$. As a consequence:

$$y(nT_e + pT_s) = h \times e^{j\theta_c^p(nT_e)} + w(nT_e + pT_s). \tag{23}$$

In that respect, by substituting (23) into (22), it ensues that

$$r_p(nT_e) = x_p(nT_e) + w_p(nT_e), \tag{24}$$

where the useful signal is equal to

$$x_p(nT_e) = h \times \left(e^{j\theta_c^p(nT_e)}\right) e^{-j\theta_c(nT_e)}, \tag{25}$$

and the noise terms are

$$w_p(nT_e) = w(nT_e + pT_s)e^{-j\theta_c(nT_e)}. \tag{26}$$

Then the complex arguments of (25) (excluding h) are given by

$$\left(-2\pi\frac{m_p}{T_s}nT_e + 2\pi BnT_e\right) \quad \text{for } n \in \left[-\frac{N}{2}, -\frac{N}{2} + \frac{m_p}{T_eB}\right),$$
$$\left(-2\pi\frac{m_p}{T_s}nT_e\right) \quad \text{for } n \in \left[-\frac{N}{2} + \frac{m_p}{T_eB}, \frac{N}{2}\right).$$

Finally, when sampling the signal at Nyquist rate $T_e = \frac{1}{B}$, we have $M = N$ and then using (19) we obtain:

$$r_p(nT_e) = h \times e^{-j2\pi\frac{m_p n}{M}} + w_p(nT_e). \tag{27}$$

Thus, $r_p(nT_e)$ is the sum of a complex exponential with normalized frequency $-\frac{m_p}{M}$ and a complex Gaussian noise. As a consequence, the Fourier transform of this discrete signal exhibits periodic peaks at the frequencies $-\frac{m_p}{N}$ mod 1, where mod means modulo. Still building upon the patent US8406275B2 [26], the optimal estimation of m_p can be performed by searching for the maximum of the periodogram of $r_p(nT_e)$, computed as $\mathcal{P}_p[k] = |R_p[k]|^2$, where $R_p[k]$, for $k \in [\![0, N-1]\!]$, is the discrete Fourier Transform (DFT) of N samples from $r_p(nT_e)$. It is expressed as follows:

$$R_p[k] = \frac{1}{\sqrt{N}} \sum_{n=-\frac{N}{2}}^{\frac{N}{2}-1} r_p(nT_e)e^{-j2\pi\frac{nk}{N}}. \tag{28}$$

Since $R_p[k]$ coincides with the Fourier transform of the finite-length discrete signal $\{r_p(nT_e)\}_{n=-N/2,\ldots,N/2-1}$ at the frequency $\frac{k}{N}$, the peak in R_p corresponding to the complex exponential at the frequency $-m_p/N$ in (27) is obtained when $k = N - m_p$. It follows that $R_p[k]$ can be expressed as:

$$R_p[k] = \sqrt{N}h\delta(k + m_p - N) + W_p[k], \tag{29}$$

where $\delta(k)$ represents the Dirac impulse, and $W_p[k]$ is the DFT of the noise. The latter keeps its statistics due to the DFT properties. To end up, the detection of m_p can be achieved by computing:

$$\hat{m}_p = N - \underset{k\in[0,N-1]}{\operatorname{argmax}} \left(\mathcal{P}_p[k]\right). \tag{30}$$

It should be noted that an equivalent all discrete description of the LoRa modulation has been proposed by [27].

III. EMPIRICAL MODELS

Physical layer performance evaluation starts with BER performance. Therefore, this section describes the empirical models and expressions used for BER analysis of RPW and LoRa as a function of carrier-to-noise ratio (CNR).

A. RPW MODEL

Analytical expressions for BER of RPW with RP-MPSK modulation is a work in progress. Therefore, simulation approach is used to evaluate BER. Q-RPW model proposed by the authors has been used for simulation of RPW communication system [3]. Let $m[n]$ be the transmitted quaternion vector, $H[n]$ the multipath quaternion coefficients vector, and $w[n]$ the quaternion noise vector, Q-RPW model is described as:

$$r[n] = m[n]H[n] + w[n] \tag{31}$$

The transmitted signal $m[n]$ is defined as

$$m[n] = \sum_{i\in\mathbb{Z}} g_i[n - iN_p] \tag{32}$$

where

$$g_i[n] = q_i e^{j\frac{2\pi n}{N_p}} \quad iN_p \le n < (i+1)N_p \tag{33}$$

is the transmitted quaternion vector of length N_p corresponding to ith quaternion symbol q_i (*see* Appendix A).

For the detection of q_i, we first rewrite (31) as:

$$r_i[n] = m_i[n]H_i[n] + w_i[n]$$

Let $\mathbf{R}$ and $\mathbf{H}$ denote the quaternion vectors corresponding to $r_i[n]$ and $H_i[n]$, respectively. The following decision metric is used for coherent detection of q_i:

$$\hat{q}_i = \underset{m}{\operatorname{argmin}}(\|\mathbf{R} - \mathbf{Z}_m\mathbf{H}\|^2), \tag{34}$$

where $\mathbf{Z}_m$ is the quaternion vector of mth correlator ($m \in [0, M-1]$), given by the following function:

$$z_m[p] = q_m e^{j\frac{2\pi p}{N_p}} \quad 0 \le p < N_p \tag{35}$$

Average number of errors N_e for transmission of N_s symbols is computed as a function of CNR to find average BER:

$$\mathrm{BER}(\Gamma) = \frac{N_e(\Gamma)}{N_s} \tag{36}$$

where Γ is the average CNR of the received signal.

B. LoRa MODEL

LoRa is a proprietary technology, and exact analytical expressions for its BER are not found in literature. However, researchers have come up with a few estimated BER expressions for LoRa [28], [29]. Closed form expression of LoRa under AWGN and Rayleigh fading conditions are proposed by Elshabrawy and Robert [29]. Their BER expression for AWGN conditions is given by:

$$P_{b,\mathrm{awgn}} = \frac{1}{2}Q(\sqrt{\Gamma \cdot 2^{SF+1}} - \sqrt{1.386 \cdot SF + 1.154}) \tag{37}$$

This empirical expression has close agreement with BER expression obtained by Reynders et al. [30] based on curve fitting of simulation results. For Rayleigh or multipath fading environment, the simplified form (*see* Appendix B) of the expression given in [29] is:

$$P_{b,\mathrm{fad}} = \frac{1}{2}Q\left(-\sqrt{a}\right) - \frac{1}{2}\exp\left(\frac{-a}{2[b+1]}\right) \times \sqrt{\frac{b}{b+1}}Q\left(-\sqrt{\frac{ab}{b+1}}\right) \tag{38}$$

where

$$a \approx 2\ln\left(2^{SF} - 1\right) + \frac{1}{(2^{SF} - 1)} + 1.15444$$
$$b = 2^{SF} \cdot \Gamma$$

IV. LINK PERFORMANCE

Link performance of RPW and LoRa is evaluated for a fixed terrestrial up-link point-to-point communication. ISM carrier frequency of 868 MHz with a 125 kHz narrowband channel for both RPW and LoRa is considered. Since most of the existing LPWANs operate on this band and existing simulations are also available for validation of the results obtained in this work [2]. Error performance is obtained as a function of CNR for both AWGN and multipath (Rayleigh fading). Because of digital modulation, the term CNR is used instead of signal-to-noise ratio (SNR) [31]. The sensitivity is obtained for an acceptable BER of 10^{-5} to limit the simulation time and compare the available BER profiles of existing LPWANs. Comparisons are given for un-coded modulations, hence no error detection or correction is employed. The reference curves for this BER range of LoRa are also available for comparison with [29]. Noise Figure (NF) of LPWANs varies between 2 to 6 dB [2], [32]. Therefore, the highest NF of this range that is 6 dB is considered in this work. Acceptable probability of fringe coverage Pr (coverage) is 0.95. Antenna heights of the GW and ED are 25 m and 8 m respectively based on and

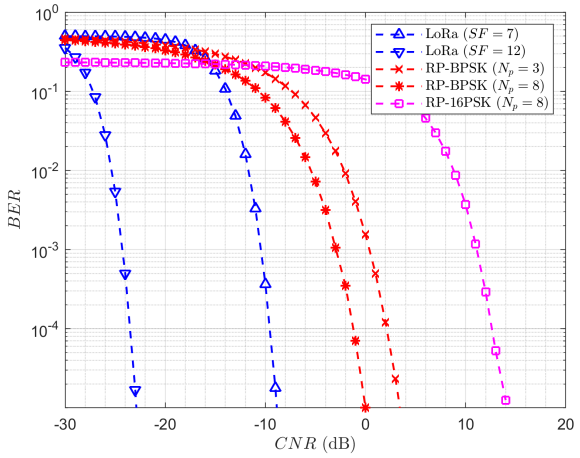

FIGURE 3. BER comparison of RPW and LoRa over AWGN.

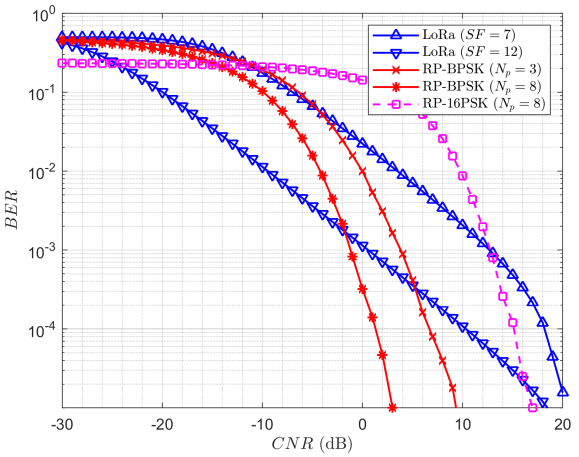

FIGURE 4. BER comparison of RPW and LoRa over rayleigh fading.

average two-level building [2]. GW antenna gain is 10 dB while ED antenna is omnidirectional. The maximum transmit power is 14 dBm which is used by unlicensed band LPWANs. Okumura-Hata propagation model is used. Shadowing and multipath fading losses are statistically estimated, and added to the path-loss obtained from Okumura-Hata model to estimate overall path loss. RSS and $R_{\max}$ are determined for urban, suburban, and rural areas. For $f_b = 125$ kHz, the bit rate R_b of RPW is 125 kbps, which is much higher than LoRa. The bit rate of LoRa is given by $R_b = B \times \mathrm{SF}/2^{\mathrm{SF}}$ [33]. With $B = 125$ kHz, and SF $= 7$ and SF $= 12$, the highest and the lowest data rate of LoRa comes out to be 6.836 kbps and 0.366 kbps, respectively. Therefore, the simulation results for three cases of RP-MPSK modulation are presented [3] for comparison with LoRa: two for RP-BPSK (lowest order RPW modulation) with $N_p = 3$ and $N_p = 8$, and the third one for RP-16PSK (highest order RPW modulation) for $N_p = 8$.

A. ERROR PERFORMANCE

Reliability is one of the most important characteristics of LPWANs. In this subsection, the BER performance of RP-BPSK and RP-16PSK modulation [5] is compared with LoRa CSS modulation under AWGN and Rayleigh fading conditions. For LoRa, the best performance is obtained for the highest spreading factor SF $= 12$ and the worst for SF $= 7$. The best case performance of LoRa is 23 dB better than that of RPW. From Fig. 3, it is evident that LoRa has an excellent BER performance for AWGN channel at about 20 dB below the noise floor (negative CNR). The key factor behind this performance is the robust CSS modulation [17]. RP-BPSK and RP-16PSK require a higher CNR for the minimum acceptable BER. RP-BPSK attains the same performance at only 0 to 4 dB above the noise floor, while a power of about 14 dB above the noise floor is required in case of RP-16PSK under AWGN conditions. The other existing demodulation methods can achieve this performance at about 8 to 10 dB above the noise floor [17].

Fig. 4 shows BER performance of LoRa and RPW with RP-BPSK and RP-16PSK modulation under multipath or Rayleigh fading conditions for the same values of SF and N_p as in Fig. 3. For lower values of CNR, LoRa performs better than RPW, however it does not satisfy the BER criteria of 10^{-5}. But for high CNR values, RPW performs significantly better than LoRa and it also satisfies the BER criteria. This is because the same RPW symbol is transmitted on all polarization angles from 0 to 2π, and received at a finite large number of polarizations N_p per symbol. It is notable that RP-BPSK with $N_p = 8$ conforms the BER criteria at a much lower CNR of 3 dB compared to 18 dB (15 dB above RPW) for LoRa with SF $= 12$. For $N_p = 3$, RP-BPSK satisfies the required BER at $\Gamma = 9$ dB. RP-16PSK achieves the same BER performance at $\Gamma = 17$ dB with $N_p = 8$. It is evident that RPW with highest order modulation RP-16PSK performs better than LoRa with highest spreading factor SF $= 12$ in terms of CNR. It is notable that RP-16PSK offers a high bit rate of 500 kbps compared to LoRa bit rate of 0.366 kbps with SF $= 12$. Therefore, RPW is more suitable for applications that demand high reliability and high transmission rate. These values along with other simulation parameters and performance specifications are given in Table 1.

TABLE 1. Simulation parameters and performance specification.

Parameter	Symbol	RP-BPSK		RP-16PSK	LoRa	
		$N_p = 3$	$N_p = 8$	$N_p = 8$	SF $= 7$	SF $= 12$
Minimum CNR-AWGN (dB)	$\Gamma_{\min}$	3	0	14	-9	-23
Minimum CNR-fading (dB)	$\Gamma_{\mathrm{f,min}}$	9	3	16.5	20	18
Fast Fading Margin (dB)	L_F	10	8	19.6	23	21
Diversity Gain (dB)	G_D	41	36	31.5	-	-
Processing Gain (dB)	G_P	-	-	-	12.62	25.33
Carrier frequency (MHz)	f_c	868				
Acceptable bit error rate	BER	1×10^{-5}				
Signal bandwidth (kHz)	B	125				
Noise Figure (dB)	NF	6				
Probability of fringe coverage	Pr(coverage)	0.95				
Location Variability (dB)	σ_L	7 (Urban), 8.4 (Suburban), 6 (Rural)				
Shadowing Margin (dB)	L_S	11.48 (Urban), 13.4 (Suburban), 9.6 (Rural)				
Antenna Gain (dBi)	G_{TX}	10				
Antenna Heights (m)	h_G, h_D	25, 8				
Uplink Transmit power (dBm)	P_t	0 to 14				
Miscellaneous losses (dB)	L_M	40				

B. SENSITIVITY

Sensitivity is the minimum received signal power to satisfy the desired BER [34]. The lower is the power, the higher is the sensitivity. If holding time of the channel is large compared

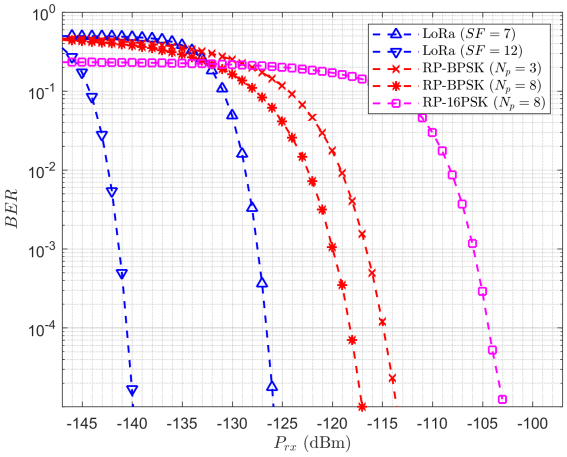

FIGURE 5. Sensitivity levels of RPW and LoRa over AWGN channel.

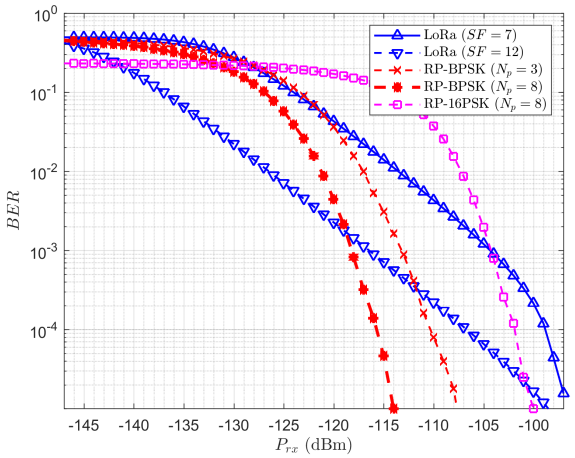

FIGURE 6. Sensitivity levels of RPW and LoRa under Rayleigh fading conditions.

to the fading duration as in voice transmission, BER under fading conditions is considered [34]. Therefore, a fade margin is determined from large-scale fading only. On the other hand, in case of data transmission, the channel holding time is short. The BER under only AWGN or static conditions is considered to find the receiver sensitivity [34]. Therefore fade margin is determined from both large-scale and small-scale fading. Since, both RPW and LoRa are considered as IoT technologies that involve data transmission only, the sensitivity under AWGN conditions is considered for this paper which is given in Fig. 5. However, sensitivity under fading conditions is also shown in Fig. 6 for reference. If NF is the receiver noise factor in dB, $\Gamma_{\min}$ is the minimum CNR in dB to achieve the desired BER, B is the channel bandwidth in kHz, the sensitivity σ in dBm is given by [32]:

$$\sigma = -174 + \mathrm{NF} + \Gamma_{\min} + 10\log_{10} B \tag{39}$$

Fig. 5 and Fig. 6 show the received power levels of RPW and LoRa for varying BERs under AWGN and multipath conditions using (39) with $\Gamma_{\min}$ and $\Gamma_{\mathrm{f,min}}$ from Table 1, respectively. To achieve BER of 10^{-5}, the sensitivity of LoRa under AWGN is much higher than RPW. The sensitivity of RP-BPSK for $N_p = 8$ is 9 dB worse than the sensitivity of LoRa for the lowest spreading factor (SF = 7). LoRa exhibits a sensitivity of -140 dBm with SF = 12 while it is -126 dBm with SF = 7. The sensitivity of RP-BPSK is -114 dBm and -117 dBm for $N_p = 3$ and $N_p = 8$, respectively. RP-16PSK exhibits a sensitivity of -103 dBm with $N_p = 8$. It can also be deduced that the variation of SF in LoRa has a significant impact on sensitivity, while varying N_p has comparatively low impact on sensitivity of RPW. Therefore, LoRa outperforms RPW in terms of sensitivity under AWGN conditions at the expense of bit rate.

In case of Rayleigh fading, RPW shows significantly higher sensitivity than LoRa. From Fig. 6, it can be observed that the sensitivity of the highest order RPW modulation, i.e., RP-16PSK ($N_p = 8$) is slightly higher than the best case of LoRa (SF = 12). Furthermore, this translates to a considerably higher bit rate of RPW (500 kbps) than LoRa (0.366 kbps), as indicated in the beginning of Section IV. Using lower order RPW modulation (RP-BPSK) instead of higher order modulation (RP-16PSK) offers an advantage of about 15 dB in sensitivity with $N_p = 8$. Therefore, it is deduced that RPW can perform reasonably well in heavy multipath environment.

C. PATH LOSS

Several factors contribute to path loss experienced by LPWANs. A path loss element is either because of large-scale fading (variation over distance) or small-scale fading (variation over time) [35] while the latter is mostly ignored in LPWAN literature. The large-scale fading is caused by

1) attenuation commonly modeled by free-space loss (FSL) or plane-earth loss (PEL),
2) obstruction losses due to edge diffraction and clutter (trees and buildings) and
3) shadowing due to clutter variation.

Empirical path loss models account for both the attenuation due to FSL or PEL and the obstruction losses due to clutter [35]. These models are generally applied to macrocells considering the effects of typical clutter on a flat or a gently rolling terrain at a given distance. However, the clutter at a given distance on one path is different from clutter at the same distance on another path [35]. It causes variations in nominal path loss obtained from empirical path loss models. Resulting variations in RSS are known as shadowing or slow fading. Shadowing is statistically characterized by a log-normal random variable that turns out to be Gaussian random variable when converted to dB, and therefore, can be added to the median path loss in dB. The small-scale fading includes multipath fading often expressed by Rayleigh or Rician distribution [35].

In this paper, Okumura-Hata model has been considered in combination with shadowing and multipath losses to determine overall path loss. Okumura-Hata is the most widely used path loss model, sometimes regarded as a standard [35]. The Okumura-Hata path loss L_{OH} is characterized by

categorizing the area as urban, suburban or rural. The overall variable path loss $\widetilde{L}_T$ [36] is given below by

$$\widetilde{L}_T = L_{OH} + \widetilde{L}_S + \widetilde{L}_F, \tag{40}$$

where $\widetilde{L}_S \sim \mathcal{N}\left(0, \sigma_L^2\right)$ measured in dB, accounts for shadowing, and $\widetilde{L}_F$ accounts for fast fading represented in logarithmic form to conform with the equation. Since (40) quantifies the variable path loss, it is necessary to establish the maximum acceptable path loss L_T to compare the link budgets allowed in RPW and LoRa on the edge of coverage by adding appropriate fade margins for shadowing and fast fading:

$$L_T = L_{OH} + L_S + L_F \tag{41}$$

The shadowing margin L_S and the fast fading margin L_F are statistically determined. The three loss elements in (41) as used in this paper are discussed in this section.

1) OKUMURA-HATA PATH LOSS MODEL

Okumura-Hata Model is widely adopted in performance evaluation of wireless systems over different terrains such as urban, suburban and open or rural areas [2]. It is given by (42), as shown at the bottom of the next page, where f_c is the carrier frequency in MHz, h_G is the gateway antenna height, h_D is the end-device antenna height, $a\left(h_D\right)$ is a function of the end-device antenna height that depends on terrain, d is the distance between gateway and end-device, and c is the correction factor which also depends on terrain. For simulation we have considered, $f_c = 868$ MHz, $h_G = 30$ m and $h_D = 8$ m. The function $a\left(h_D\right)$ is given by (43), as shown at the bottom of the next page, and the correction factor c is determined by (44), as shown at the bottom of the next page.

2) SHADOWING LOSS

Signal depolarization in highly reflective and cluttered environments can be mitigated if polarization diversity is used [37]. RPW is an efficient polarization diversity technique because of its ability to trail the severity of depolarization. Experiments carried out by Hitachi Research Laboratories have shown successful transmission of RPW signal through a small hole of the drawer in which the transceiver prototype was placed. Thus it can better withstand shadowing compared to LoRa. Equal shadowing margin is considered for both RPW and LoRa in this paper. The shadowing margin L_S is calculated from the log-normal shadowing $\widetilde{L}_S$ in dB as

$$\widetilde{L}_S = \sigma_L \cdot z, \tag{45}$$

where, σ_L is the standard deviation of $\widetilde{L}_S$, known as location variability, and $z \sim \mathcal{N}(0, 1)$ [35]. The location variability depends on f_c, h_G, h_D and the environment. It is greatest in suburban areas and lowest in open and rural areas. In case of sub-GHz carriers, it falls between 6 to 9 dB [35]. An empirical expression for σ_L to conform with Okumura-Hata Model [38] is given by

$$\sigma_L = 0.65\left[\log f_c\right]^2 - 1.3\log f_c + A, \tag{46}$$

where A is the environment-dependent location variability parameter. For urban areas, $A = 5.2$, and for suburban areas, $A = 6.6$ [38]. Since, the lowest value of σ_L in LPWANs is 6 dB that corresponds to open and rural areas as mentioned above, a tentative approximation of A for rural areas is 4.2. Putting the values of A into (46), the approximate value of σ_L for urban and suburban areas is 7 dB and 8.4 dB, respectively. Now the probability of a minimum increase of L_S dB in median path loss L_{OH} due to shadowing at a given distance can be calculated as [35]:

$$\Pr\left(\widetilde{L}_S > L_S\right) = Q\left(\frac{L_S}{\sigma_L}\right) = Q\left(z_L\right) \tag{47}$$

Here, $Q(\cdot)$ is known as the tail of cumulative normal distribution and $1 - Q(\cdot)$ gives the probability of successful communication at the fringe of coverage [35]. The right-hand side of (47) is obtained from (45) by substituting $\widetilde{L}_S = L_S$ and $z = z_L$. We use inverse of Q function (Q^{-1}) to find shadowing margin L_S:

$$L_S = \sigma_L Q^{-1}\left[1 - \Pr\left(\text{coverage}\right)\right] \tag{48}$$

For this paper, we have considered 95% successful coverage, so that $L_S \approx 1.64\sigma_L$.

3) FAST FADING

Fast fading is one of the major contributors to overall path loss encountered by a communication link. Fast fading loss can be worse than shadowing. The fade margin L_F associated with fast fading [19] can be estimated as

$$L_F = 10 \cdot \log\left[-\ln\left(1 - P_{\text{out}}\right)\right], \tag{49}$$

where P_{out} is the probability that BER exceeds the minimum acceptable BER under Rayleigh conditions [39] given by

$$P_{\text{out}} = \frac{1}{2}\left(1 - \sqrt{\frac{\Gamma_{\text{f,min}}}{2 + \Gamma_{\text{f,min}}}}\right), \tag{50}$$

and $\Gamma_{\text{f,min}}$ is the minimum required CNR to maintain desired quality of communication under Rayleigh fading conditions. From Fig. 4, $\Gamma_{\text{f,min}}$ for LoRa is 63 while it is 2 in case of RPW on linear scale, and hence P_{out} is 0.0077 and 0.1467, respectively. Putting these values into (49) gives respective L_F values of 21 dB and 8 dB. A list of simulation parameters and performance specification calculated above is given in Table 1. Fig. 7 shows the maximum acceptable path loss L_T of RPW and LoRa for urban, suburban and rural areas using (41). This is the first work on path loss of RPW, however, the curves for LoRa agree with the results reported in [2] except the fade margins have been added for distances up to 50 km.

It is interesting to note that RP-16PSK ($N_p = 8$) suffers almost the same path loss as LoRa (SF = 12). This is a

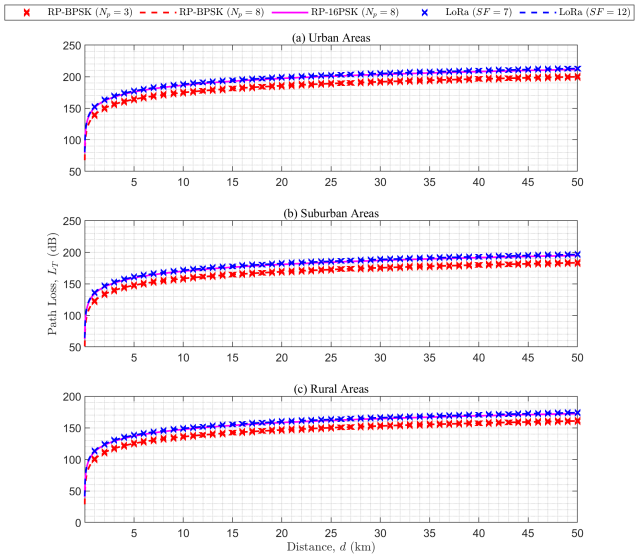

FIGURE 7. Total path loss of RPW and LoRa in (a) urban areas, (b) suburban areas, and (c) rural areas.

significant result as RP-16PSK has a much higher bit rate than LoRa (SF = 12). It can also be noticed that LoRa performs 13 dB worse than RP-BPSK. This difference arises from the enhanced resilience of RPW to fading channels. As expected, the smallest path loss was obtained in rural areas, and the largest in urban areas. Path loss in rural areas is 160 and 173 dB for RP-BPSK and LoRa respectively, and an approximate additional loss of 20 dB each is incurred going from rural to suburban, and suburban to urban areas. These values also show the same trend as reported in [2]. Path loss values of RP-BPSK, RP-16PSK and LoRa for all three environments are given in Table 2.

D. RECEIVED SIGNAL STRENGTH

In order to find RSS, we use the following expression:

$$\text{RSS} = P_t + G_T - L_T, \tag{51}$$

Here P_t is the transmit power, G_T is the sum of all gains, and L_T is the sum of all losses. For RPW, the diversity gain, and for LoRa, the processing gain due to spread spectrum technique must be included to overall gain in (51). The description of effective RPW gain and LoRa processing gain and some other losses is given in below:

1) EFFECTIVE RPW GAIN

The performance advantage of a diversity scheme is two-folds: diversity gain and array gain [40]. Diversity gain is only defined under fading conditions and it corresponds to the increase in the slope of BER versus CNR curve. Equivalently, the difference between average output CNR of a diversity-less system and that of a diversity system keeps on increasing with increasing CNR [41]. Array gain, also called power gain, is defined for AWGN channel as the increase in average output CNR relative to the single branch average CNR [40]. These two gains provide an overall gain in the average output CNR. Since noise is uncorrelated with the signal in our case, we define effective RPW gain G_d as the ratio of average output CNR of single branch ideal BPSK system to that of RP-BPSK system for a given BER under Rayleigh fading condition:

$$G_d = \frac{\Gamma_{\text{ideal}}}{\Gamma_{\text{f,min}}}, \tag{52}$$

Here $(\cdot)_d$ denotes gain on linear scale, and Γ_{ideal} is the minimum CNR for ideal BPSK modulation on linear scale to satisfy the stated conditions. Effective RPW gain is controlled by setting the sampling ratio N_p according to the requirements. As indicated above in Fig. 4, for sampling ratio of $N_p = 8$ and BER of 10^{-5}, $\Gamma_{\text{f,min}} = 3$ dB for RP-BPSK. On the other hand, from the theoretical BER performance of BPSK over fading channel, we find that $\Gamma_{\text{ideal}} = 44$ dB. These values translate to effective RPW gain $G_D = 41$ dB, where capital subscript $(\cdot)_D$ denotes gain in dB. Similarly, it can be shown that for RP-16PSK, $G_D = 31$ dB.

2) LoRa PROCESSING GAIN

The amount of spreading in LoRa depends on the ratio of chip rate R_c to bit rate R_b. The processing gain G_p of LoRa [33] on linear scale is computed by

$$G_p = \frac{2^{\text{SF}}}{\text{SF}}. \tag{53}$$

For the highest spreading factor (SF = 12), $G_P = 25.33$ dB, where $(\cdot)_P$ denotes gain in dB.

In addition to the gains described above, the gateway (GW) antenna gain G_{TX} of 10 dB is also accounted in link budget calculation [20]. Also, the obstruction losses and indoor losses are taken into account as already discussed.

$$L_{OH} = 69.55 + 26.16\log f_c - 13.82\log h_G - a(h_D) + \left[44.9 - 6.55\log h_G\right]\log d - c \tag{42}$$

$$a(h_D) = \begin{cases} 3.2[\log(11.75h_D)]^2 - 4.97 & \text{for urban areas} \\ 1.1\log f_c - 0.7h_D - [1.56\log f_c - 0.8] & \text{for suburban and rural areas} \end{cases} \tag{43}$$

$$c = \begin{cases} 4.78\,(\log f_c)^2 - 18.33\log f_c + 40.94 & \text{for rural and open areas areas} \\ 2\left[\log\left(\frac{f_c}{28}\right)\right]^2 + 5.4 & \text{for suburban areas} \\ 0 & \text{for urban areas} \end{cases} \tag{44}$$

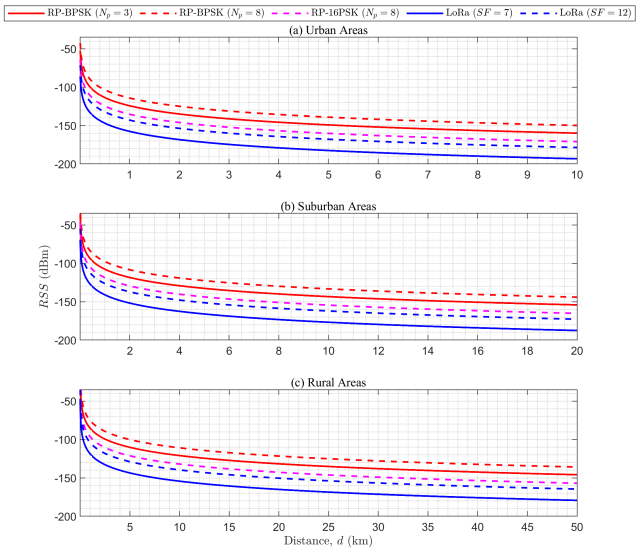

FIGURE 8. RSS of RPW and LoRa in (a) Urban Areas (b) Suburban Areas (c) Rural Areas.

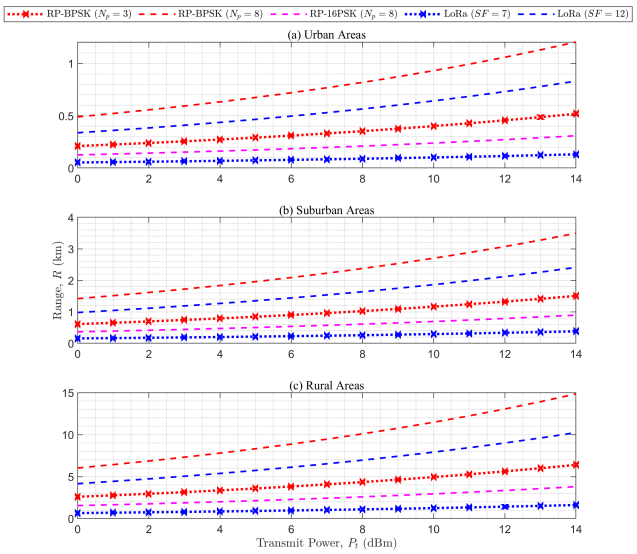

FIGURE 9. Maximum Range of RPW and LoRa in (a) Urban Areas (b) Suburban Areas (c) Rural Areas.

After G_D and G_P are known, we replace $G_T = G_D + G_{RX}$ for RPW, and $G_T = G_P + G_{RX}$ for LoRa into (51) to find the link budget. The gains calculated above are listed in Table 1.

Two other losses have been considered in this paper as miscellaneous losses L_M. They are fixed obstruction losses [2] often caused by obstructive terrains not tackled in macrocell path loss models, and indoor penetration loss [20]. A loss of 20 dB on 868 MHz was used in [2]. Since these losses are also frequency dependent, the same value is taken into account for comparison of LoRa and RPW. The latter includes the outdoor-indoor attenuation at building boundaries and indoor obstruction losses. Indoor loss of 10, 20 and 30 dB was used in [20]. A 20 dB loss is selected in this paper.

Fig. 8 shows RSS of RPW and LoRa in urban, suburban and rural areas. We consider a reference distance of 100 m (a typical Wi-Fi coverage fringe) to compare the values of RPW and LoRa in the three environments. RSS of RP-16PSK ($N_p = 8$) is approximately 7 dB higher than LoRa (SF = 12). It can be observed that RSS of RP-BPSK ($N_p = 8$) is about 29 dB stronger than LoRa (SF = 12) for all three environments. RP-BPSK ($N_p = 3$) overtakes LoRa (SF = 7) by 33 dB. However, RSS of both LoRa and RPW is improved by 40 dB while going from urban to rural areas. Comparative values of RSS are given in Table 2 for further reference.

E. RANGE

The maximum range of a communication system is the distance it can cover with highest transmit power and minimum RSS. Therefore, we replace RSS $= \sigma$ in (51) and solve for d to find the maximum range $R_{\max}$ considering all gains and losses discussed above:

$$R_{\max} = 10^{\frac{P_t + G_T + \sigma - y_1 + y_2 + k_t - L_X}{b_h}} \tag{54}$$

Here $L_X = L_S + L_F + L_M$ is the total excess loss. This equation is similar in form to the range equation given in [2], but it presents a more accurate description of range with the exponent accounting for some additional gains and losses. Other parameters involved in (54) are defined [2] as

$$y_1 = 69.55 + 26.16 \log f_c, \quad y_2 = 13.82 \log h_G,$$
$$k_t = a(h_D) + c_t, \quad b_h = 44.9 - 6.55 \log h_G.$$

Fig. 9 shows comparative range of RPW and LoRa in urban, suburban and rural areas. RP-16PSK ($N_p = 8$) covers longer range than LoRa (SF = 7), but shorter than both RP-BPSK ($N_p = 3, 8$) and LoRa (SF = 12). However, in all three environments, RP-BPSK outperforms LoRa. With the maximum transmit power of 14 dBm, the maximum range achieved by RP-BPSK is 15 km in rural areas which is 5 km longer than LoRa under the same propagation conditions. The difference is relatively small in case of urban and suburban areas. Compared to 0.8 km and 2.4 km range of LoRa in urban and suburban areas, the maximum range of RP-BPSK is 1.2 km and 3.5 km respectively. We conclude that the range of RPW is at least 1.5 times higher than LoRa in general. The overall range of RPW for worst case performance ($N_p = 3$) is at least four times longer than LoRa (SF = 12). More values are given in Table 2 for an excessive comparison. For validation, the results in Fig. 9 can be cross-checked for agreement with [2]. For example, only antenna gain (9 dB) on GW end is considered for LoRa in [2] with a sensitivity of -137 dBm. However, we have considered the processing gain $G_P = 25.33$ dB in addition to GW antenna gain $G_{RX} =$ 10 dB, with a sensitivity of -140 dBm for LoRa. On the other hand, the total excess loss of LoRa is contributed by cable loss (3 dB), fixed obstacle loss (20 dB) and variable obstacle loss (28.1 dB) in [2], while in this paper, we consider shadowing margin ($L_S = 11.5$ dB) for urban areas, fading margin ($L_F = 21$ dB), fixed obstacle loss (20 dB) and indoor

TABLE 2. Comparison of link performance.

Performance Measure	Symbol	RPW (RP-BPSK)		RP-16PSK	LoRa	
		$N_p = 3$	$N_p = 8$	$N_p = 8$	SF = 7	SF = 12
Sensitivity-AWGN (dBm)	σ	-114	-117	-103	-126	-140
Sensitivity-Fading (dBm)	σ	-108	-114	-100	-97	-99
Link Budget (dB)	-	128	131	117	140	154
Data Rate (kbps)	R_b	125	125	125	6.836	0.366
Maximum Path Loss (dB)	L_T	200 (urban) 183 (suburban) 161 (rural)		211 195 172	213 196 174	
Received Signal Strength (dBm) (100 m)	RSS	-88 (urban) -72 (suburban) -49 (rural)	-78 -62 -39	-100 -83 -61	-121 -105 -83	-107 -91 -68
Maximum Range (km)	$R_{\max}$	0.52 (urban) 1.5 (suburban) 6.4 (rural)	1.2 3.5 14.8	0.31 0.9 3.8	0.13 0.38 1.6	0.83 2.4 10.2

loss (20 dB) to find the maximum range of LoRa. This leads to a significant advantage of 7.95 dB in LoRa received power in this paper. Similar crosschecks can be performed to verify the performance in suburban and rural areas.

V. SUMMARY OF RESULTS

In this subsection we summarize the comparative performance of RPW and LoRa. Table 2 lists six aspects of performance namely sensitivity, total path loss, link budget, data rate, received signal strength, and range, spanning over best- and worst-case values for three different propagation environments. The primary advantage of LoRa is its higher sensitivity than RPW, allowing more link budget. However, it must be noted that LoRa has performance limitations in multipath environment, therefore, more fade margin is required to establish a successful communication link. It can also be concluded that that RP-BPSK performs significantly better than LoRa, while RP-16PSK can perform equivalent to LoRa. In both cases, the bit rate of RPW is much higher than LoRa. BER performance also shows that RPW outperforms LoRa by a substantial margin, making it a robust and and reliable LPWAN technology. Therefore, RPW is a more viable solution for critical IoT applications that demand high data rate and high reliability.

VI. CONCLUSION

This paper is the first performance comparison of LoRa and the emerging RPW LPWAN over a point-to-point link further categorized into urban, suburban, and rural scenarios. Sensitivity, shadowing and fast fading margins for RPW and LoRa are statistically estimated using known techniques instead of empirical measurements. It can also be deduced that the variation of SF in LoRa has a significant impact on sensitivity, while varying N_p has comparatively low impact on sensitivity of RPW. Effective gain of RPW is defined and computed from BER curve for link budget considerations. Range of RPW and LoRa is determined and compared for all three types of environment and was found to be in close agreement with existing literature under given conditions. Results have shown an overall advantage of RPW over LoRa on a point-to-point link with a longer range.

Future works on this comparison include the coverage analysis in remote areas and forests, spectral and energy efficiency, and studying the effects of depolarization.

APPENDIX A DERIVATION OF QUATERNION RP-MPSK SYMBOL

A dual-polarized transmitter transmits two complex symbols s_H and s_V through HP and VP antennas, respectively, as

$$s_H = a_H + \iota\, b_H \text{ and } s_V = a_V + \iota b_V,$$

where $(s_H \perp s_V)$ and $a_H, b_H, a_V, b_V \in R$. Like the real and imaginary parts of a complex number on a complex plane, the resultant q of the above pair of constellations can be represented as a quaternion [14]:

$$q = s_H + j s_V = a_H + b_H\iota + a_V j + b_V\kappa \tag{55}$$

Equation (55) represents a quaternion or a three-dimensional complex symbol, where ι, j, κ are hyper-complex numbers having the following characteristics according to the definition of quaternion [14]:

$$\iota^2 = j^2 = \kappa^2 = \iota j\kappa = -1$$
$$\iota j = -j\iota = \kappa, j\kappa = -\kappa j = \iota, \kappa\iota = -\iota\kappa = j$$

Equation (55) can be further generalized to describe an arbitrary polarization state of a plane wave [14]. If the polarization is rotated by an angle φ with respect to HP, the new polarization state q_φ can be expressed as

$$q_\varphi = q e^{j\varphi} = (s_H + j s_V)(\cos\varphi + j\sin\varphi) \tag{56}$$

Any change in polarization, e.g. due to polarization mismatch or depolarization, will also appear as a factor in (56).

For RPW transmission, since two MPSK modulations are performed side-by-side with a quadrature phase difference as mentioned in Section II, the corresponding HP and VP symbols to be transmitted at ith time instant satisfy the condition $s_V = s_H e^{(\iota\pi/2)}$. Therefore, (55) takes the form

$$q_i = s_i[1 + e^{\iota\pi/2}] = a_i + b_i\iota - b_i j + a_i\kappa \tag{57}$$

where $s_i = a_i + b_i\iota$ is the ith MPSK symbol, and q_i is the RP-MPSK symbol with initial polarization that rotates through 2π radians in N_p steps results in a vector $g_i[n]$ with elements of the form (56), given below:

$$g_i[n] = q_i e^{j\frac{2\pi n}{N_p}}$$

APPENDIX B SIMPLIFIED EXPRESSION OF LoRa EMPIRICAL BER

The empirical BER expression proposed by Elshabrawy and Robert [29] is

$$P_b \approx \frac{1}{2}Q\left(-\sqrt{2H_{2^{SF}-1}}\right) - \frac{1}{2}\sqrt{\frac{2^{SF}\Gamma}{2^{SF}\Gamma+1}}\exp\left(\frac{2H_{2^{SF}-1}}{2\left(2^{SF}\Gamma+1\right)}\right) \times Q\left(\sqrt{\frac{2^{SF}\Gamma+1}{2^{SF}\Gamma}}\left[-\sqrt{2H_{2^{SF}-1}} + \frac{\sqrt{2H_{2^{SF}-1}}}{2^{SF}\Gamma+1}\right]\right)$$

where $H_{2^{SF}-1} \approx \ln 2^{SF} - 1 + \frac{1}{2(2^{SF}-1)} + 0.57722$. Let

$$a \approx 2\ln\left(2^{SF}-1\right) + \frac{1}{(2^{SF}-1)} + 1.15444$$
$$b = 2^{SF} \cdot \Gamma$$

So that we can rewrite as

$$P_b = \frac{1}{2}Q(-\sqrt{a}) - \frac{1}{2}\sqrt{\frac{b}{b+1}}\exp\left(-\frac{a}{2(b+1)}\right) \times Q\left(\sqrt{\frac{b+1}{b}}\left[-\sqrt{a} + \frac{\sqrt{a}}{b+1}\right]\right)$$

Simplification of the argument of second $Q(\cdot)$ function results in

$$P_{b,\text{fad}} = \frac{1}{2}Q\left(-\sqrt{a}\right) - \frac{1}{2}\exp\left(\frac{-a}{2[b+1]}\right) \times \sqrt{\frac{b}{b+1}}Q\left(-\sqrt{\frac{ab}{b+1}}\right)$$

ACKNOWLEDGMENT

The authors acknowledge the help and support extended by the Hitachi Research Laboratories, Japan, and the University of Bordeaux, France.

CONFLICT OF INTEREST

All authors declare that they have no conflict of interest. This paper does not contain any studies with human participants or animals performed by any of the authors.

REFERENCES

[1] (2020). *Number of LPWAN Connections by Technology Worldwide From 2017 to 2023*. [Online]. Available: https://www.statista.com/statistics/880822/lpwan-ic-market-share-by-technology/
[2] A. Ikpehai, B. Adebisi, K. M. Rabie, K. Anoh, R. E. Ande, M. Hammoudeh, and H. Gacanin, "Low-power wide area network technologies for Internet-of-Things: A comparative review," *IEEE Internet Things J.*, vol. 6, no. 2, pp. 2225–2240, Apr. 2019.
[3] Z. Ahmad, S. J. Hashim, F. Z. Rokhani, S. A. R. Al-Haddad, A. Sali, and K. Takei, "Quaternion model of higher-order rotating polarization wave modulation for high data rate M2M LPWAN communication," *Sensors*, vol. 21, no. 2, pp. 1–18, Jan. 2021.
[4] N. S. Chilamkurthy, O. J. Pandey, A. Ghosh, L. R. Cenkeramaddi, and H.-N. Dai, "Low-power wide-area networks: A broad overview of its different aspects," *IEEE Access*, vol. 10, pp. 81926–81959, 2022.
[5] Z. Ahmad, S. J. Hashim, F. Z. Rokhani, S. A. R. Al-haddad, and A. Sali, "Enhanced rotating polarization wave for robust wireless connectivity," in *Proc. 9th IFIP/IEEE Int. Conf. Perform. Eval. Model. Wired Wireless Netw.*, Berlin, Germany, Dec. 2020, pp. 1–6.
[6] Z. Ahmad, S. J. Hashim, F. Z. Rokhani, S. A. R. Al-Haddad, and A. Sali, "LPWAN state of the art: Trends and future directions," in *Proc. Smart City Conf.* India: IIT Madras, 2021.
[7] R. K. Kalle, "Reliable and prioritized communication using polarization diversity for industrial Internet of Things," in *Proc. IEEE Conf. Wireless Sensors (ICWiSE)*, Oct. 2016, pp. 89–94.
[8] S. Vitturi, C. Zunino, and T. Sauter, "Industrial communication systems and their future challenges: Next-generation Ethernet, IIoT, and 5G," *Proc. IEEE*, vol. 107, no. 6, pp. 944–961, Jun. 2019.
[9] A. E. Ferreira, F. M. Ortiz, L. H. M. K. Costa, B. Foubert, I. Amadou, and N. Mitton, "A study of the Lora signal propagation in forest, urban, and suburban environments," *Ann. Telecommun.*, vol. 75, nos. 7–8, pp. 333–351, Aug. 2020.
[10] J. A. Azevedo and F. E. Santos, "A model to estimate the path loss in areas with foliage of trees," *AEU Int. J. Electron. Commun.*, vol. 71, pp. 157–161, Jan. 2017.
[11] A. S. Adegoke, "Measurement of propagation loss in trees at SHF frequencies," Ph.D. dissertation, Dept. Elect. Electron. Eng., Univ. Leicester, Leiceser, U.K., 2014.
[12] Y. S. Meng, Y. H. Lee, and B. C. Ng, "Empirical near ground path loss modeling in a forest at VHF and UHF bands," *IEEE Trans. Antennas Propag.*, vol. 57, no. 5, pp. 1461–1468, May 2009.
[13] K. Staniec and M. Kowal, "LoRa performance under variable interference and heavy-multipath conditions," *Wireless Commun. Mobile Comput.*, vol. 2018, pp. 1–9, Apr. 2018.
[14] L. Emmanuel, W. Farjow, and X. Fernando, "LoRa wireless link performance in multipath underground mines," in *Proc. Int. Conf. Innov. Intell. for Informat., Comput., Technol. (ICT)*, Sep. 2019, pp. 1–4.
[15] Embedded Staff. (2017). *Optimizing LoRa Radio Performance for Embedded Devices*. [Online]. Available: https://www.embedded.com/optimizing-lora-radio-performance-for-embedded-devices/
[16] V. A. Dambal, S. Mohadikar, A. Kumbhar, and I. Guvenc, "Improving LoRa signal coverage in urban and sub-urban environments with UAVs," in *Proc. Int. Workshop Antenna Technol. (iWAT)*, Mar. 2019, pp. 210–213.
[17] A. Jebril, A. Sali, A. Ismail, and M. Rasid, "Overcoming limitations of LoRa physical layer in image transmission," *Sensors*, vol. 18, no. 10, p. 3257, Sep. 2018.
[18] M. Cattani, C. Boano, and K. Römer, "An experimental evaluation of the reliability of LoRa long-range low-power wireless communication," *J. Sensor Actuator Netw.*, vol. 6, no. 2, p. 7, Jun. 2017.
[19] K. S. Zaidi, V. Jeoti, M. Drieberg, A. Awang, and A. Iqbal, "Fading characteristics in evaporation duct: Fade margin for a wireless link in the South China Sea," *IEEE Access*, vol. 6, pp. 11038–11045, 2018.
[20] M. Lauridsen, H. Nguyen, B. Vejlgaard, I. Z. Kovacs, P. Mogensen, and M. Sorensen, "Coverage comparison of GPRS, NB-IoT, LoRa, and SigFox in a 7800 km area," in *Proc. IEEE 85th Veh. Technol. Conf. (VTC Spring)*, Jun. 2017, pp. 3–7.
[21] B. Sklar, *Digital Communications: Fundamentals and Applications*, 2nd ed. London, U.K.: Pearson, 2001.
[22] C. Oestges and B. Clerckx, *MIMO Wireless Communications: From Real-World Propagation to Space-Time Code Design*. New York, NY, USA: Academic, 2007.
[23] H. Yamada and K. Takei, "Highly-reliable rotating polarization wave transceiver with optimal polarization selection," *Proc. IEEE Radio Wireless Symp. (RWS)*, Jan. 2019, pp. 1–3.
[24] B. Buurman, J. Kamruzzaman, G. Karmakar, and S. Islam, "Low-power wide-area networks: Design goals, architecture, suitability to use cases and research challenges," *IEEE Access*, vol. 8, pp. 17179–17220, 2020. [Online]. Available: https://ieeexplore.ieee.org/document/8963911/
[25] O. B. A. Seller and N. Sornin, "Low power long range transmitter," U.S. Patent 9 252 834, Feb. 2, 2016.
[26] F. Sforza, "Communication Systems," U.S. Patent 8 406 275, Mar. 26, 2013.
[27] L. Vangelista, "Frequency shift chirp modulation: The LoRa modulation," *IEEE Signal Process. Lett.*, vol. 24, no. 12, pp. 1818–1821, Dec. 2017.
[28] G. Ferre and A. Giremus, "LoRa physical layer principle and performance analysis," in *Proc. 25th IEEE Int. Conf. Electron., Circuits Syst. (ICECS)*, Dec. 2018, pp. 65–68.
[29] T. Elshabrawy and J. Robert, "Closed-form approximation of LoRa modulation BER performance," *IEEE Commun. Lett.*, vol. 22, no. 9, pp. 1778–1781, Sep. 2018.
[30] B. Reynders, W. Meert, and S. Pollin, "Range and coexistence analysis of long range unlicensed communication," in *Proc. 23rd Int. Conf. Telecommun. (ICT)*, May 2016, pp. 1–6. [Online]. Available: http://ieeexplore.ieee.org/document/7500415/
[31] (2012). *C/N Ratio(CNR) Versus S/N Ratio(SNR)-Difference Between CNR and SNR*. [Online]. Available: https://www.rfwireless-world.com/Terminology/Carrier_to_Noise_Ratio_versus_Signal_to_Noise_Ratio.html
[32] Y. Roth, J.-B. Doré, L. Ros, and V. Berg, "The physical layer of low power wide area networks: Strategies, information theory's limit and existing solutions," *Adv. Signal Process., Rev.*, vol. 1, pp. 1–29, Sep. 2018.
[33] *LoRa Modulation Basics AN1200.22*, Semtech, Camarillo, CA, USA, 2015, pp. 1–26.
[34] V. K. Garg, *Wireless Communications and Networking*, 1st ed. San Francisco, CA, USA: Elsevier, 2007.
[35] S. R. Saunders and A. A. Zavala, *Antennas and Propagation for Wireless Communication Systems*, 2nd ed. Mississauga, ON, Canada: Wiley, 2007.
[36] *How to Include Rayleigh Fading Into Path Loss Model?* Electrical Engineering Stack Exchange. Accessed: May 18, 2021. [Online]. Available: https://electronics.stackexchange.com/questions/311821/how-to-include-rayleigh-fading-into-path-loss-model

[37] J. Frolik, "Mitigating severe channel effects using tripolar antenna diversity," in *Proc. 9th Eur. Conf. Antennas Propag. (EuCAP)*, 2015, pp. 1–4.
[38] Y. Okumura, E. Ohmori, T. Kawano, and K. Fukuda, "Field strength and its variability in VHF and UHF land-mobile radio service," *Rev. Electr. Commun. Laboratories*, vol. 16, pp. 825–873, Jan. 1968.
[39] Q. M. Qadir, "Analysis of the reliability of LoRa," *IEEE Commun. Lett.*, vol. 25, no. 3, pp. 1037–1040, Mar. 2021.
[40] B. Clerckx and C. Oestges *MIMO Wireless Networks: Channels, Techniques and Standards for Multi-Antenna, Multi-User and Multi-Cell Systems*, 2nd ed. Waltham, MA, USA: Elsevier, 2013.
[41] M. K. Simon, *Digital Communication Over Fading Channels*, 2nd ed. Hoboken, NJ, USA: Wiley, 2005.

ZAID AHMAD (Member, IEEE) received the B.S. degree in communication systems engineering from the Institute of Space Technology, Pakistan, in 2007, and the M.S. degree in telecommunication from Iqra University, Pakistan, in 2012. He is currently pursuing the Ph.D. degree with the Department of Computer and Communication Systems Engineering, Universiti Putra Malaysia (UPM). He is also a Lecturer at COMSATS University (CUI), Pakistan. His research interests include wireless communication, the IoT, physical and MAC layers, and machine-to-machine (M2M) communication.

SHAIFUL J. HASHIM received the B.Eng. degree in electrical and electronics engineering from the University of Birmingham, U.K., in 1998, the M.Sc. degree from the National University of Malaysia, in 2003, and the Ph.D. degree from Cardiff University, U.K., in 2011. He is currently a Professor at the Department of Computer and Communication Systems Engineering, Faculty of Engineering, Universiti Putra Malaysia (UPM). He has contributed to more than 100 technical and research publications. His research interests include the Internet of Things (IoT), software-defined networking (SDN), network security, cloud computing, and non-linear wireless measurement systems.

GUILLAUME FERRÉ (Senior Member, IEEE) graduated in electronic and telecommunication engineering (ENSIL) from the University of Limoges, France, in 2003. He received the Ph.D. degree in digital communications and signal processing from the Limoges University of Technology, in 2006. From 2006 to 2008, he was a Postdoctoral Researcher with the Limoges XLIM Laboratory and then at the IMS Laboratory, Bordeaux. Since 2008, he has been an Associate Professor at ENSEIRB-MATMECA, an engineering school of Bordeaux INP. After several administrative responsibilities with the Telecommunications Department, ENSEIRB-MATMECA, where he is currently the Director of industrial relations. He carries out his research activities at the IMS Laboratory with the "Signal and Image" Team. These fields of research concern the circuits and systems for digital communications, including signal processing and digital communications for 5G and the IoT, digital enhancement for wideband power amplifiers, and time interleaved analog to digital converters. He is the principal investigator (PI) of many national and international projects. At the local level, he is responsible for two research activities related to the IoT, including one to investigate on the smart campus. He is the author of more than 100 papers in international conferences. He is also the author of seven patents. He is a member of several Technical Program Committees, such as ICT and ICECS.

FAKHRUL Z. ROKHANI (Member, IEEE) is currently affiliated with the Department of Computer and Communication Systems Engineering, University Putra Malaysia, where he is currently working as a Lecturer. He has published numerous publications in various national and international peer-reviewed journals and presented scientific articles across the world. His clinical and scientific research interest includes embedded systems. Because of the active association with different societies, academies, and contributions, he is recognized by the subject experts around the world. His contributions are appreciated by various reputed awards.

S. A. R. AL-HADDAD (Senior Member, IEEE) received the Ph.D. degree in electrical, electronic and systems engineering from the National University Malaysia. He started as a Lecturer at the Department of Computer and Communications Systems Engineering, Universiti Putra Malaysia, in 1997, and was promoted as an Associate Professor and a Professor, in 2012 and 2020, respectively. He has taught students of undergraduate and graduate programs, and secured international and national grants. He has a few patents and copyrights on his name. His special interests include human and animal sound processing, Al-Quran sound processing, media security, and biometric systems. He has been an Active Member of professional societies, such as the past Chair of IEEE SMC Malaysia Chapter and the past Chairperson IT of the National Islamic Calligraphy.

ADUWATI SALI (Senior Member, IEEE) received the B.Eng. degree in electrical electronics engineering (communications) from The University of Edinburgh, U.K., in 1999, the M.Sc. degree in communications and network engineering from Universiti Putra Malaysia (UPM), Malaysia, in April 2002, and the Ph.D. degree in mobile and satellite communications from the University of Surrey, U.K., in July 2009. She worked as an Assistant Manager with Telekom Malaysia Bhd, from 1999 to 2000. She was the Deputy Director at the UPM Research Management Centre (RMC), where she was responsible for research planning and knowledge management, from 2016 to 2019. She has been a Professor at the Department of Computer and Communication Systems, Faculty of Engineering, UPM, since February 2019. She is also a Chartered Engineer (C.Eng.) registered under the U.K. Engineering Council and a Professional Engineer (P.Eng.) under the Board of Engineers Malaysia (BEM). She is involved with IEEE as the Chair to ComSoc/VTS Malaysia (2017 and 2018) and Young Professionals (YP) (2015); and the Young Scientists Network-Academy.